

# Designing slower glasses by manipulating their local structure

Susana Marín Aguilar, Henricus H. Wensink, Giuseppe Foffi,\* and Frank Smallenburg†  
*Laboratoire de Physique des Solides, CNRS, Université Paris-Sud, Université Paris-Saclay, 91405 Orsay, France*  
(Dated: March 26, 2025)

Glasses remain an elusive and poorly understood state of matter. For example, it is not clear how we can design an efficient macroscopic glass former by tuning the properties of its microscopic building blocks. In this paper, we propose a simple directional colloidal model that reinforces the optimal icosahedral local structure of binary hard-sphere glasses. We show that only this specific symmetry results in a dramatic slowing down of the dynamics. Our results open the door to controlling the dynamics of dense glassy systems by selectively promoting specific local structural environments.

When we cool down or compress a liquid sufficiently rapidly to avoid crystallization, we end up with a glass: a dynamically arrested state which lacks long-range order. Glasses are ubiquitous in condensed matter and can be found in fields of great technological interest, including materials science, biomaterials, food science, and polymer physics. Although the transition from a fluid into a glass is dramatic from a dynamics perspective, it is accompanied by surprisingly little structural change: based on purely structural information, it is hard to tell whether a system has reached dynamical arrest or not [1, 2]. The non-ergodic nature of glasses breaks the fundamental assumptions of equilibrium statistical mechanics and, as a consequence, it is extremely difficult to understand the microscopic origin of the glass transition. For this reason, the bottom-up design of a good glass former is not a trivial task. It is well understood, for example, that glassy dynamics are accompanied by the emergence of long-lived locally favored structures (LFS) [3–7]. However, these are always found a posteriori, by investigating models that are known to be good glass formers. In order to aid our understanding of the microscopic mechanisms behind glass formation, it would be extremely useful to identify the ingredients required to design building blocks with a maximized propensity for facilitating dynamical arrest.

In this Letter, we explore the glass scenario of particles decorated with attractive patches on their surface, interpolating between the extreme cases of pure hard spheres and short-ranged attractive particles. Both these models have been widely studied experimentally, numerically and theoretically for their high-density glassy behavior [8–12]. In particular, short-ranged attractive potentials display a remarkable reentrant glassy behavior [11–18], in which the glass first speeds up and then slows down again upon cooling. Our directional model is inspired by the growing experimental availability of patchy colloidal particles [19–23]. The ability of these particles to form well-defined directional bonds allows them to self-assemble into open crystal structures [24, 25] and (at low densities) into strong network-forming glasses [22, 26, 27]. We propose to use the directionality of patchy particles as an ideal tool for pinning down the role of LFS in the

vitrification of dense glasses.

Here, we use extensive computer simulations to demonstrate that directional interactions can be designed which selectively promote the LFS responsible for dynamical arrest. Specifically, we show that the glassy dynamics of patchy systems are remarkably independent of the number and geometry of the patches, with the notable exception of the icosahedral 12-patch geometry. Due to their ability to match and reinforce the icosahedral local structure in the hard-sphere fluid, 12-patch particles are uniquely capable of facilitating dynamical arrest. In this sense, the 12-patch particles represent the most effective glass former that can be designed.

To model the patchy interactions, we follow the Kern-Frenkel model [28] and model the particles as hard spheres, decorated with  $n$  attractive patches each. In order to suppress crystallization, we simulate a binary mixture of Kern-Frenkel particles of two sizes, with the size ratio given by  $\sigma_S/\sigma_L = 0.833$ , where  $\sigma_{L(S)}$  denotes the size of the large (small) spheres. Two attractive patches form a bond with bonding energy  $\epsilon$  when they overlap. The size of each patch is controlled by an opening angle  $\theta$  and a fixed maximum interaction range  $r_c = 1.031\sigma_{ij}$ , where  $\sigma_{ij}$  is the contact distance between particles  $i$  and  $j$ . This interaction range was chosen to be consistent with the square-well interaction in Ref. 16. Here, we study systems with 3, 4, 6, 8, 12, and 20 patches, with the patches uniformly distributed over the surface, as illustrated in Fig. 1. We restrict our model to only allow a single bond for any pair of particles, even if multiple patches on the same particle overlap. With this restriction, the model interpolates between the hard-sphere model at  $\theta = 0$  and the square-well model when  $\theta$  is larger than a critical  $\theta_f$  where the patches cover the entire sphere surface. To simulate these particles, we use event-driven molecular dynamics (EDMD) simulations [26, 29]. In each system, we fix the number of particles  $N = 700$ , the composition  $x = 0.5$ , and the packing fraction  $\eta = 0.58$ . In Ref. 16, it was shown that this square-well system at this packing fraction has a clear reentrance as a function of temperature. Note that we report all dynamical quantities for the large particles only. For the small particles, the behavior is qualitatively the

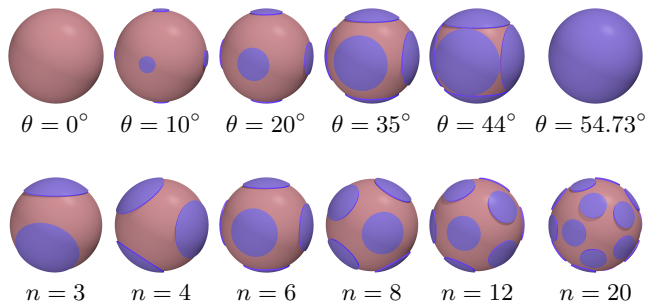


FIG. 1. Illustration of the simulation model. The top row shows particles with 6 attractive patches with varying patch sizes determined by the opening angle  $\theta$ . The bottom row shows the patch geometry for different numbers of patches, corresponding to the vertices of a triangle ( $n = 3$ ), tetrahedron ( $n = 4$ ), octahedron ( $n = 6$ ), square antiprism ( $n = 8$ ), icosahedron ( $n = 12$ ), and dodecahedron ( $n = 20$ ).

same.

We begin our analysis by investigating whether the reentrant behavior of the diffusion coefficient as a function of temperature persists in the presence of directional interactions. To this end, we measure the dimensionless diffusion coefficient  $D\tau/\sigma_L^2$ , where  $\tau = \sqrt{\beta m \sigma_L^2}$  is our time unit, with  $\beta = 1/k_B T$ ,  $k_B$  Boltzmann's constant,  $T$  the temperature, and  $m$  the mass of a particle. In Fig. 2a, we show this diffusion coefficient for systems with  $n = 6$  patches, as a function of the reduced temperature  $k_B T/\epsilon$ , for a number of different values of the patch angle  $\theta$ . In the limit of high  $\theta$ , we recover the case of an isotropic square-well model in the glassy regime, and find reentrant diffusive behavior [16, 30], where the system crosses over from an attractive glass to a repulsive one. Upon decreasing  $\theta$ , we observe an overall decrease in the diffusion, as shown in Fig. 2a, which retains its reentrant behavior as observed in a recent mean-field solution for a simpler patch geometry [31]. However, the maximum in the diffusion rate shifts to lower temperatures as  $\theta$  decreases. This behavior can be understood from the observation that particles with lower coverage fractions form fewer bonds, implying that lower temperatures are required before bonding to similarly affect the dynamics. In the case of 12-patch particles (Fig. 2b) we see a similar decrease in diffusivity with decreasing patch size, but the shift in the maximum is less pronounced. We observe similar trends for the other patch geometries we explored.

In order to explore the effect of the patch geometry in more detail, we now fix the total fraction of the particle surface covered by the patches to 40%, and measure the diffusion constant as a function of the patch geometry. The results are shown in Fig. 3a. Surprisingly, we see that the diffusion coefficient is largely independent of the patch geometry, except for the case of 12 patches, where we instead see an extreme slowdown of the system at low temperature. Note that in the 20-patch case, the

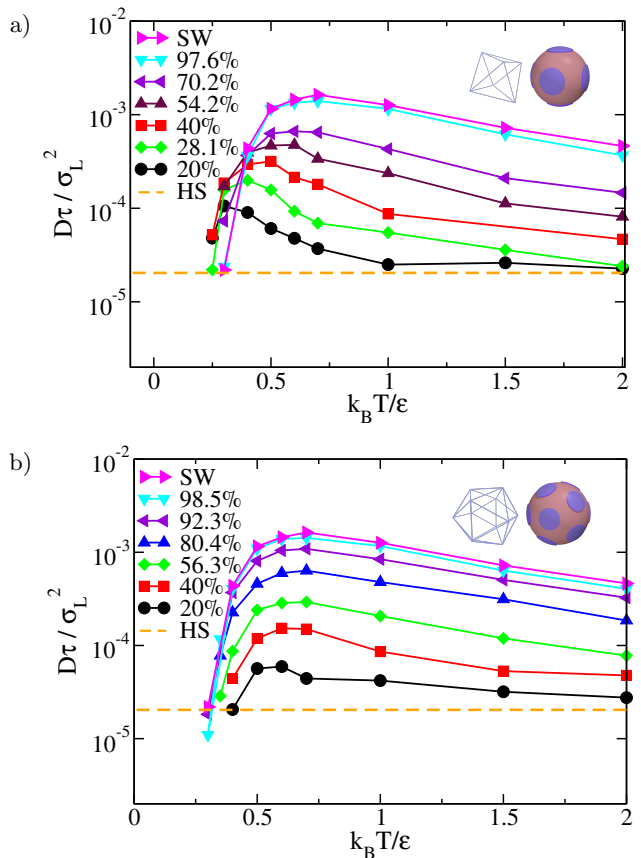


FIG. 2. Translational diffusion coefficient calculated for a system of 6 patches (a) and 12 patches (b). The star lines correspond to the HS and the SW limit. The reentrance is conserved until low angles, where the system behaves like a mixture of HS.

system crystallizes at temperatures  $k_B T/\epsilon \lesssim 0.4$  into the CsCl structure, which is compatible with the 20-patch geometry (see SI).

In order to make a more complete analysis of the dynamics, we measure in each system the density correlation function  $F(q, t)$ , which characterizes the relaxation time in the system at different length scales, given the wave vector  $q$ . In Fig. 3b, we plot these correlation functions for temperature  $k_B T/\epsilon = 0.4$ , at the value of  $q$  corresponding to the first peak in the structure factor. We observe an approximate collapse of the correlation functions for the 3, 4, 6, 8, and 20-patch cases, with the 12-patch system as a single outlier which relaxes much more slowly. We define the relaxation time  $\tau_{0.3}$  as the time at which the correlation function decays to 0.3. To confirm that the collapse of correlation functions is independent of  $q$ , we plot in Fig. 3c the relaxation times as a function of  $q$ . Clearly, all systems with a number of patches other than 12 relax at approximately the same rate, regardless of the length scale. Interestingly, at this temperature, the relaxation dynamics of the 12-patch particles are over an order of magnitude slower than all other geometries,

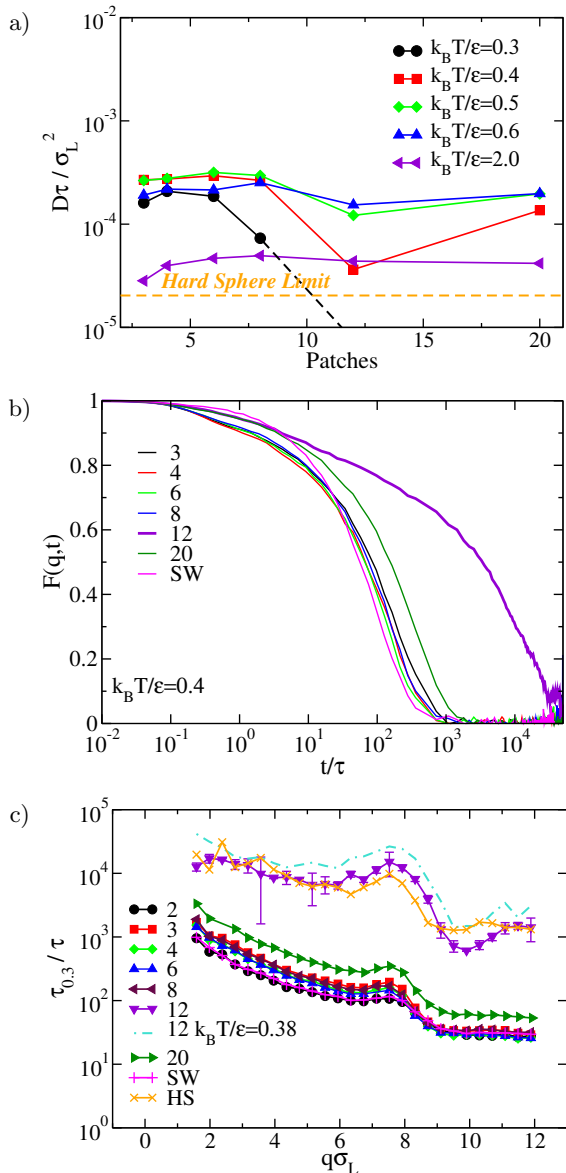


FIG. 3. a) Diffusion coefficient as a function of number of patches, at different temperatures, for patchy particles with a fixed overall patch coverage fraction 40%. Note that for the 12-patch system at  $k_B T/\epsilon = 0.3$ , the system could not be equilibrated, and hence the dashed lines connect to an approximate result. b) Density correlation function of the same systems, for a wavevector  $q$  corresponding to the first peak of the structure factor, at fixed temperature  $k_B T/\epsilon = 0.4$ . c) Wave vector dependence of the relaxation time  $\tau_{0.3}$ , at the same temperature. The dashed line shows the results for a 12-patch system at a slightly lower temperature  $k_B T/\epsilon = 0.38$ .

and closely match those of a hard-sphere system. Note, however, that at even lower temperatures, the 12-patch system continues to slow down rapidly. To illustrate this, in Fig. 3c we also include data for the 12-patch system at  $k_B T/\epsilon = 0.38$  (dashed line), where the dynamics have clearly slowed down beyond the hard-sphere case. Our

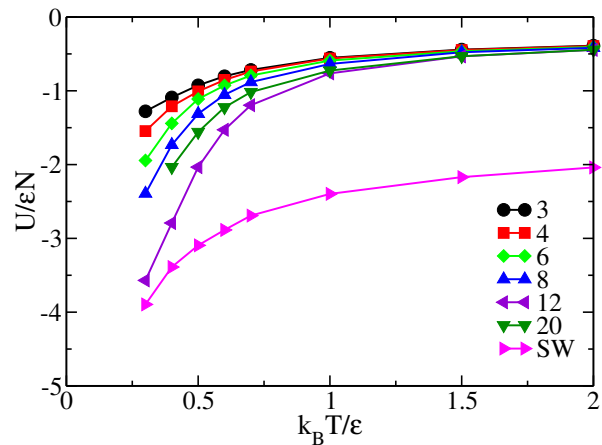


FIG. 4. Energy per particle  $U/\epsilon N$  as a function of temperature for different patch geometries, with a fixed patch coverage fraction of 40%. SW indicates the square-well system.

exploration of even lower temperatures is limited by the rapid increase of required simulation lengths.

To shed more light on the exceptionally slow dynamics of the 12-patch system, we turn our attention to the number of bonds formed in the system. In Fig. 4, we plot the potential energy  $U$  as a function of temperature for the different patch geometries, as well as the square-well system. Note that low potential energy indicates a large number of bonds. As one might expect, in the patchy system bonds start forming in large numbers at significantly lower temperatures in comparison to the square-well system. This is consistent with the overall shift to lower  $T$  of the dynamical features (Fig. 2) at lower coverage fractions. Interestingly, the 12-patch system forms more bonds than all other patchy systems, and closely approaches the number of bonds of the square-well system at low temperatures. This strongly suggests that the 12-patch geometry is more compatible with the local structure of the cages in the hard-sphere glass.

Hence, to fully understand the dynamical arrest in our system, we now focus on the local structure of the glass. We note that the 12 patches on each particle are arranged in an icosahedral geometry. Recent literature has demonstrated that icosahedral order is an important contributor to slow dynamics in glassy systems, including hard spheres [32]. Additionally, it has been argued that local order matching the structure of a (meta)stable crystal phase in the system plays a particularly important role in dynamical slowing down [33]. For binary hard-sphere mixtures with a size ratio around 0.833, the stable crystal structures in the phase diagram include single-component face-centered cubic (FCC) crystals, as well as the binary Laves phase  $MgZn_2$  [34], which contains multiple icosahedral motifs in its structure. However, the composition  $x = 0.5$  of our system is incompatible with the stoichiometry of the Laves phase, implying that a large-scale

demixing is needed for macroscopic crystallization to take place, which does not occur in our simulations. However, the stability of the Laves phase does suggest that icosahedral order is an important locally favored structure in the hard-sphere mixture under consideration, similar to the case of the Wahnström mixture, which stabilizes the same crystal structure [32, 35].

In order to confirm this hypothesis, we analyze the local structure of our systems using local bond order parameters  $Q_6$  and  $\hat{W}_6$  as they are explained in Refs. 36 and 37. These local order parameters characterize the environment of each particle, based on its nearest neighbors. For a perfect icosahedral cage,  $Q_6 = 0.663$  and  $\hat{W}_6 = -0.170$ . These values provide a reference point for finding icosahedral structure in the glass. We classify all particles whose environment is sufficiently similar to this ideal cage (i.e.  $Q_6 > 0.5$  and  $\hat{W}_6 < -0.1$ ), as icosahedral particles, as illustrated in the inset of Fig. 5. We then plot in Fig. 5 the fraction  $N_{\text{ico}}/N$  of icosahedral particles in the system as a function of temperature for different patch geometries. In the hard-sphere limit (corresponding to high temperatures), we find that approximately 20% of particles are in an icosahedral environment. Lowering the temperature initially decreases this number for all patch geometries, as well as for a pure square-well system, indicating that the formation of a small number of short-ranged bonds disrupts local icosahedral order. However, in the case of the square-well system, icosahedral order suddenly increases rapidly at  $k_B T/\epsilon \lesssim 0.4$ , signalling the emergence of highly bonded icosahedral clusters. In the 12-patch system, this increase already occurs at much higher temperatures, and is more extreme: at the lowest temperatures investigated the number of icosahedral environments has approximately doubled in comparison to the hard-sphere limit.

Glasses of short-ranged attractive colloids in the high density regime have been shown to display a set of unexpected properties that have been intensely debated in the last twenty years [11–18, 30]. At the time, the interest was exclusively on isotropic interactions. To our knowledge, this paper provides the first numerical study of the glass behaviour of dense patchy colloidal systems. We find that the reentrant melting, typical of short-ranged attractive colloids, is preserved irrespective of the number of patches and their size. Moreover, for particles with 12 patches arranged on the vertices of an icosahedron, the formation of icosahedral cages in the glass is enhanced, creating a more strongly arrested glass, with longer relaxation times. In contrast, for other patch geometries with the same surface coverage fraction, the number of patches and their location does not play a crucial role in setting the dynamical time scales.

We attribute this striking dynamical effect to the fact that icosahedral particles match the long-lived local icosahedral structure responsible for caging in the repulsive glass [32, 33]. In contrast, the dynamical speedup

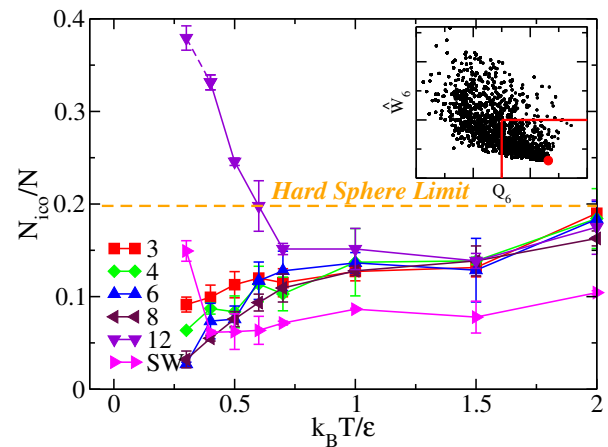


FIG. 5. Fraction of particles in a local environment with icosahedral order, as a function of temperature and patch geometry. The dashed horizontal line indicates the value in the hard-sphere limit. The inset shows a plot of the bond order parameters  $Q_6$  and  $\hat{W}_6$  for individual 12-patch particles at  $k_B T/\epsilon = 0.3$ , with the red dot indicating the values corresponding to a perfect icosahedral cage. The particles in the region delimited by the red lines are considered to be in an icosahedral environment.

that occurs at intermediate temperatures for all patch geometries can be at least partly be interpreted as stemming from a disruption of the icosahedral cages of the repulsive glass. Evidently, the effect of interactions on glass forming ability hinges on their interplay with locally favored structures. By designing particles that inherently promote the formation of “slow” local environments, we provide a clear recipe for creating the most effective glass former.

We thank Francesco Sciortino for useful discussions. S. Marín Aguilar acknowledges CONACyT for funding.

\* giuseppe.foffi@u-psud.fr

† frank.smallenburg@u-psud.fr

- [1] L. Berthier and G. Biroli, *Rev. Mod. Phys.* **83**, 587 (2011).
- [2] G. L. Hunter and E. R. Weeks, *Rep. Prog. Phys.* **75**, 066501 (2012).
- [3] G. Tarjus, S. A. Kivelson, Z. Nussinov, and P. Viot, *J. Phys.: Condens. Matter* **17**, R1143 (2005).
- [4] J. E. Hallet, F. Turci, and P. Royall, *Nat. Commun.* **9**, 3272 (2018).
- [5] A. Malins, J. Eggers, C. P. Royall, S. R. Williams, and H. Tanaka, *J. Chem. Phys.* **138**, 12A535 (2013).
- [6] C. P. Royall and S. R. Williams, *Phys. Rep.* **560**, 1 (2015).
- [7] C. P. Royall and W. Kob, *J. Stat. Mech.: Theo. Exp.* **2017**, 024001 (2017).
- [8] E. R. Weeks, J. C. Crocker, A. C. Levitt, A. Schofield, and D. A. Weitz, *Science* **287**, 627 (2000).
- [9] L. Berthier, G. Biroli, J.-P. Bouchaud, L. Cipelletti, D. E.

- Masri, D. L'Hôte, F. Ladieu, and M. Pierno, *Science* **310**, 1797 (2005).
- [10] L. Berthier, D. Coslovich, A. Ninarello, and M. Ozawa, *Phys. Rev. Lett.* **116**, 238002 (2016).
- [11] K. N. Pham, A. M. Puertas, J. Bergenholtz, S. U. Egelhaaf, A. Moussaid, P. N. Pusey, A. B. Schofield, M. E. Cates, M. Fuchs, and W. C. Poon, *Science* **296**, 104 (2002).
- [12] G. Foffi, K. A. Dawson, S. V. Buldyrev, F. Sciortino, E. Zaccarelli, and P. Tartaglia, *Phys. Rev. E* **65**, 050802 (2002).
- [13] J. Bergenholtz and M. Fuchs, *Phys. Rev. E* **59**, 5706 (1999).
- [14] K. Dawson, G. Foffi, M. Fuchs, W. Götze, F. Sciortino, M. Sperl, P. Tartaglia, T. Voigtmann, and E. Zaccarelli, *Phys. Rev. E* **63**, 011401 (2000).
- [15] A. M. Puertas, M. Fuchs, and M. E. Cates, *Phys. Rev. Lett.* **88**, 098301 (2002).
- [16] E. Zaccarelli, G. Foffi, K. A. Dawson, S. V. Buldyrev, F. Sciortino, and P. Tartaglia, *Phys. Rev. E* **66**, 041402 (2002).
- [17] T. Eckert and E. Bartsch, *Phys. Rev. Lett.* **89**, 125701 (2002).
- [18] K. N. Pham, S. U. Egelhaaf, P. N. Pusey, and W. C. K. Poon, *Phys. Rev. E* **69**, 011503 (2004).
- [19] R. M. Choueiri, E. Galati, H. Thérien-Aubin, A. Klinkova, E. M. Larin, A. Querejeta-Fernández, L. Han, H. L. Xin, O. Gang, E. B. Zhulina, *et al.*, *Nature* **538**, 79 (2016).
- [20] G.-R. Yi, D. J. Pine, and S. Sacanna, *J. Phys.: Condens. Matter* **25**, 193101 (2013).
- [21] V. Meester, R. W. Verweij, C. van der Wel, and D. J. Kraft, *ACS Nano* **10**, 4322 (2016).
- [22] S. Biffi, R. Cerbino, G. Nava, F. Bomboi, F. Sciortino, and T. Bellini, *Soft Matter* **11**, 3132 (2015).
- [23] I. I. Smalyukh, *Annu. Rev. Condens. Matter Phys.* **9**, 207 (2018).
- [24] W. Liu, M. Tagawa, H. L. Xin, T. Wang, H. Emamy, H. Li, K. G. Yager, F. W. Starr, A. V. Tkachenko, and O. Gang, *Science* **351**, 582 (2016).
- [25] Q. Chen, S. C. Bae, and S. Granick, *Nature* **469**, 381 (2011).
- [26] F. Smallenburg and F. Sciortino, *Nat. Phys.* **9**, 554 (2013).
- [27] C. De Michele, S. Gabrielli, P. Tartaglia, and F. Sciortino, *J. Phys. Chem. B* **110**, 8064 (2006).
- [28] N. Kern and D. Frenkel, *J. Chem. Phys.* **118**, 9882 (2003).
- [29] L. Hernández de la Peña, R. van Zon, J. Schofield, and S. B. Opps, *J. Chem. Phys.* **126**, 074105 (2007).
- [30] F. Sciortino, *Nat. Mater.* **1**, 145 (2002).
- [31] H. Yoshino, arXiv preprint arXiv:1807.04095 (2018).
- [32] C. P. Royall, A. Malins, A. J. Dunleavy, and R. Pinney, *J. Non-Cryst. Solids* **407**, 34 (2015).
- [33] M. Leocmach and H. Tanaka, *Nat. Commun.* **3**, 974 (2012).
- [34] A.-P. Hynninen, L. Filion, and M. Dijkstra, *J. Chem. Phys.* **131**, 064902 (2009).
- [35] U. R. Pedersen, T. B. Schrøder, J. C. Dyre, and P. Harrowell, *Phys. Rev. Lett.* **104**, 105701 (2010).
- [36] P. J. Steinhardt, D. R. Nelson, and M. Ronchetti, *Phys. Rev. B* **28**, 784 (1983).
- [37] Y. Wang, S. Teitel, and C. Dellago, *J. Chem. Phys.* **122**, 214722 (2005).